A half-metallic A- and B-site-ordered quadruple perovskite oxide CaCu3Fe2Re2O12 with large magnetization and a high transition temperature

nature COMMUNICATIONS

ARTICLE

Received 31 Jan 2014 | Accepted 17 Apr 2014 | Published 22 May 2014

DOI: 10.1038/ncomms4909

A half-metallic A- and B-site-ordered quadruple perovskite oxide $CaCu_3Fe_2Re_2O_{12}$ with large magnetization and a high transition temperature

Wei-tin Chen[1,†], Masaichiro Mizumaki[2], Hayato Seki[1], Mark S. Senn[3,†], Takashi Saito[1], Daisuke Kan[1], J. Paul Attfield[3] & Yuichi Shimakawa[1,4]

Strong correlation between spins and conduction electrons is key in spintronic materials and devices. A few ferro- or ferrimagnetic transition metal oxides such as $La_{1-x}Sr_xMnO_3$, Fe_3O_4, CrO_2 and Sr_2FeMoO_6 have spin-polarized conduction electrons at room temperature, but it is difficult to find other spin-polarized oxides with high Curie temperatures (well above room temperature) and large magnetizations for spintronics applications. Here we show that an A- and B-site-ordered quadruple perovskite oxide, $CaCu_3Fe_2Re_2O_{12}$, has spin-polarized conduction electrons and is ferrimagnetic up to 560 K. The couplings between the three magnetic cations lead to the high Curie temperature, a large saturation magnetization of 8.7 μ_B and a half-metallic electronic structure, in which only minority-spin bands cross the Fermi level, producing highly spin-polarized conduction electrons. Spin polarization is confirmed by an observed low-field magnetoresistance effect in a polycrystalline sample. Optimization of $CaCu_3Fe_2Re_2O_{12}$ and related quadruple perovskite phases is expected to produce a new family of useful spintronic materials.

[1] Institute for Chemical Research, Kyoto University, Uji, Kyoto 611-0011, Japan. [2] Japan Synchrotron Radiation Research Institute, SPring-8, Sayo, Hyogo 679-5198, Japan. [3] Centre for Science at Extreme Conditions and School of Chemistry, University of Edinburgh, Mayfield Road, Edinburgh EH9 3JZ, UK. [4] Japan Science and Technology Agency, CREST, Uji, Kyoto 611-0011, Japan. † Present addresses: Center for Condensed Matter Sciences, National Taiwan University, Roosevelt Road, Taipei 10617, Taiwan (W.-t.C.); Diamond Light Source Ltd., Harwell Science and Innovation Campus, Didcot OX11 0DE, UK (M.S.S.). Correspondence and requests for materials should be addressed to Y.S. (email: shimak@scl.kyoto-u.ac.jp).

Materials with spin-polarized conduction electrons are of considerable interest in magnetic and electronic materials' research and for technological applications such as spin-polarized field emission and spin-polarized tunnelling devices[1]. The Heusler alloy NiMnSb was the first predicted half-metallic ferromagnet[2], and the oxides CrO_2 (refs 3,4) and Fe_3O_4 (refs 5,6) also have half-metallic electronic structures and were intensively investigated. Discovery of colossal magnetoresistances in perovskite (for example, $La_{1-x}Sr_xMnO_3$) and pyrochlore (for example, $Tl_2Mn_2O_7$) manganese oxides cast further light on the importance of strong correlations of spins and electrons in half-metallic transition metal oxides[7–10]. In the hole-doped Mott insulator $La_{1-x}Sr_xMnO_3$, double exchange between Mn^{3+} and Mn^{4+} mediated by the itinerant holes results in ferromagnetic spin ordering[11–13] and a half-metallic electronic band structure[14,15]. The high spin polarization of conduction electrons enabled novel spintronic devices to be developed, for example, a spin-dependent tunnelling trilayer structure where tunnelling conduction depends on the spin polarization of two electrodes[16–18]. This leads to large tunnelling magnetoresistance (TMR) in a low magnetic field, which can be exploited in high-performance magnetic sensors and extremely high-density memories. Although a large TMR was observed in such trilayer devices at low temperatures, the TMR ratio became small at room temperature because the degree of spin polarization decreases significantly near the magnetic transition temperature. Materials that have highly spin-polarized conduction electrons at room temperature and hence a magnetic transition temperature well above 300 K are therefore very desirable for further spintronic developments.

Transition metal oxides with an ordered double-perovskite structure $A_2BB'O_6$, where the transition metal ions B and B′ are arranged alternately in a rock-salt manner[19–21], are useful materials for spintronic applications[22,23]. An important example is Sr_2FeMoO_6, which is half-metallic and shows substantial TMR at room temperature[24]. The B-site Fe^{3+} ($3d^5$, $S=5/2$) and the B′-site Mo^{5+} ($4d^1$, $S=1/2$) spins couple antiferromagnetically, leading to ferrimagnetism. Below the magnetic transition temperature ($T_c=410$ K) only the minority-spin bands, which mainly consist of Fe 3d t_{2g} and Mo 4d t_{2g} orbitals hybridized with O 2p orbitals, cross the Fermi level (E_F), producing spin-polarized conduction electrons. A recent Monte Carlo study of Sr_2FeMoO_6 showed that the electron spin polarization is proportional to the core spin magnetization and depends on temperature and disorder[25,26]. We have explored a strategy for enhancing spintronic properties relative to double perovskites by introducing further magnetic cations that can participate in a 1:3 order at the A sites, leading to the discovery of a new A- and B-site ordered quadruple perovskite oxide with large magnetization and a high magnetic ordering temperature.

The A- and B-site-ordered quadruple perovskite-structure oxide is derived from the A-site-ordered perovskite with general formula $AA'_3B_4O_{12}$, which consists of a framework with heavily in-phase tilted BO_6 octahedra and $A'O_4$ squares[21]. Unlike the A site in the basic ABO_3 perovskites, which is usually occupied by alkali-metal, alkaline-earth or rare-earth cations, the A′ site in $AA'_3B_4O_{12}$ can accommodate transition metal ions. The introduction of A′–A′ and A′–B magnetic interactions in addition to B–B couplings gives rise to a variety of intriguing properties[27,28]. For example, in $CaCu_3B_4O_{12}$ materials with $A'=Cu^{2+}$ and nonmagnetic ions at the B site, the A′–A′ interaction is ferromagnetic for B = Ge and Sn but antiferromagnetic for B = Ti[29,30]. When magnetic species like Mn are introduced into the B sites, the A′(Cu)–B(Mn) antiferromagnetic interaction becomes dominant and ferrimagnetism is observed in $ACu_3Mn_4O_{12}$ for A = Ca, La and Bi[31–33]. In the present study we prepared an $AA'_3B_2B'_2O_{12}$ A- and B-site-ordered quadruple perovskite oxide to explore whether the advantages of an A-site-ordered $AA'_3B_4O_{12}$ perovskite and an $A_2BB'O_6$ double perovskite can be combined. The $AA'_3B_2B'_2O_{12}$ crystal structure consists of 1:3 ordered A and A′ cations and rock-salt-ordered B and B′ cations (Fig. 1). A few compounds with this structure type were already known, but none are half-metallic. $CaCu_3Cr_2Sb_2O_{12}$ and $CaCu_3Fe_2Sb_2O_{12}$ have nonmagnetic Sb^{5+} ions at the B′ site so antiferromagnetic A′(Cu^{2+})–B(Cr^{3+}/Fe^{3+}) interactions are dominant and these materials are ferrimagnetic insulators with T_c's of 160 and 170 K, respectively[34,35]. In contrast, $CaCu_3Cr_2Ru_2O_{12}$ is metallic but shows Pauli-paramagnetic behaviour[36]. We have explored other materials in which both B-site cations have potentially mobile d electrons that may give rise to half-metallic ground states for spintronic applications, resulting in the discovery of $CaCu_3Fe_2Re_2O_{12}$, which has highly spin-polarized conduction electrons and is ferrimagnetic with a large magnetization up to $T_c=560$ K.

Results

Crystal structure of $CaCu_3Fe_2Re_2O_{12}$. A polycrystalline sample of $CaCu_3Fe_2Re_2O_{12}$ was obtained by synthesis under a high pressure (10 GPa) and high temperature (1400 K), as described in Methods. The sample was confirmed from synchrotron X-ray diffraction (SXRD) to be single phase and crystallized in a cubic $2a_0\times2a_0\times2a_0$ A-site-ordered perovskite structure. ($a_0\approx4$ Å is the lattice constant of a simple perovskite ABO_3.) Observation of (h k l) reflections with odd h, k, l values evidences rock-salt-type ordering of the B and B′ cations with $Pn\bar{3}$ space group symmetry. These B-site-ordering superstructure SXRD peaks were found to be broad compared with the fundamental reflections (which have even values of $h+k+l$). This shows that the B-site Fe/Re ordering does not extend over the full scale of the crystallites, and the Fe/Re ordering coherence length was estimated to be $\approx$140 nm (190 unit cell lengths) from modelling the broadening with a Scherrer term in the Rietveld fit. No apparent oxygen off-stoichiometry was observed and the oxygen site occupancy was set to be unity in the refinement. The high X-ray scattering contrast between Fe and Re enabled precise B-site occupancies to be determined, from which a small inversion

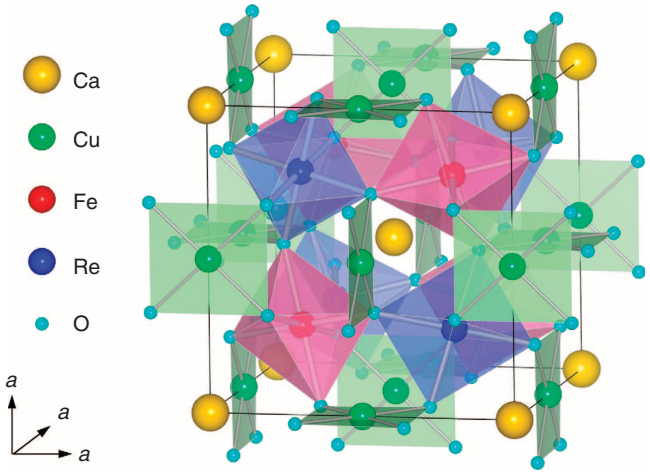

Figure 1 | Crystal structure of the A- and B-site-ordered quadruple perovskite $CaCu_3Fe_2Re_2O_{12}$. Ca and Cu ions are ordered in a 1:3 ratio at the A sites and Fe and Re ions are ordered in a rock-salt-type arrangement on the B sites of the ABO_3 perovskite structure, resulting in a framework of CuO_4 square units and heavily tilted FeO_6 and ReO_6 octahedra.

disorder of 6.2(1)% was found. The SXRD structure refinement thus confirms that $CaCu_3Fe_2Re_2O_{12}$ has the quadruple perovskite structure with well-ordered A- and B-site cations. The fit is shown in Fig. 2 and the refined structure parameters and bond distances are listed in Tables 1 and 2.

Four of the 12 Cu–O distances are short, 2.006(5) Å, revealing the square-planar coordination of oxygen around the A′ site, and the resulting distortion leads to heavy tilting of the FeO_6 and ReO_6 octahedra. The cation valence states estimated from the observed cation–oxygen bond distances by a bond valence sum method[37] are shown in Table 2. The bond valence sum values are very close to the formal values in the formula $Ca^{2+}Cu^{2+}{}_3Fe^{3+}{}_2Re^{5+}{}_2O_{12}$. The charge difference between Fe^{3+} and Re^{5+} results in the high degree of rock-salt-type cation ordering at the B/B′ sites. The same formal charge distribution was observed in $CaCu_3Fe_2Sb_2O_{12}$ (ref. 35) and in the low-temperature charge-ordered phase of $CaCu_3Fe_4O_{12}$ where B-site charge disproportionation below 210 K stabilizes the $Ca^{2+}Cu^{2+}{}_3Fe^{3+}{}_2Fe^{5+}{}_2O_{12}$ configuration[38].

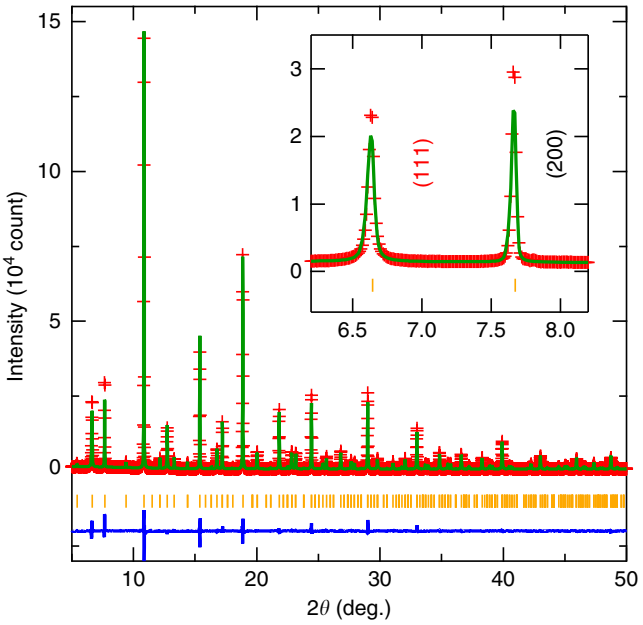

Figure 2 | Fit to the SXRD pattern of $CaCu_3Fe_2Re_2O_{12}$ at room temperature. Observed intensity points (crosses), the calculated profile (full curve) and the difference between the observed and calculated intensities (offset curve below) are shown. The ticks indicate the Bragg peak positions. The inset shows an expanded view of the low-angle (1 1 1) and (2 0 0) diffraction peaks from which additional Scherrer broadening of (1 1 1) due to limited-range coherence of Fe/Re cation order is seen.

Magnetic properties of $CaCu_3Fe_2Re_2O_{12}$. Magnetization measurements for $CaCu_3Fe_2Re_2O_{12}$ are shown in Fig. 3. A high-temperature Curie transition is observed at $T_c = 560$ K, below which a large magnetization develops with a saturation value of 8.7 μ_B per formula unit (f.u.) at 5 K. Spins from the Cu^{2+} ($3d^9$, $S = 1/2$), Fe^{3+} ($3d^5$, $S = 5/2$) and Re^{5+} ($5d^2$, $S = 1$) ions all contribute to the net magnetization of $CaCu_3Fe_2Re_2O_{12}$. Ferromagnetic $Cu^{2+}(\uparrow)$–$Fe^{3+}(\uparrow)$–$Re^{5+}(\uparrow)$ alignment of the spins gives an ideal saturated magnetization of 17 μ_B f.u.$^{-1}$, neglecting orbital contributions, while the collinear ferrimagnetic combinations $Cu^{2+}(\downarrow)$–$Fe^{3+}(\uparrow)$–$Re^{5+}(\uparrow)$, $Cu^{2+}(\uparrow)$–$Fe^{3+}(\uparrow)$–$Re^{5+}(\downarrow)$ or $Cu^{2+}(\uparrow)$–$Fe^{3+}(\downarrow)$–$Re^{5+}(\uparrow)$ are respectively predicted to give 11, 9 or 3 μ_B f.u.$^{-1}$. The observed saturated magnetization of 8.7 μ_B f.u.$^{-1}$ is thus close to the ferrimagnetic $Cu^{2+}(\uparrow)$–$Fe^{3+}(\uparrow)$–$Re^{5+}(\downarrow)$ value.

Ferromagnetic coupling between Cu^{2+} and Fe^{3+} moments was confirmed by magnetic circular dichroism (MCD) intensities from X-ray absorption spectroscopy (XAS) measurements at 15 K, as shown in Fig. 4. The observed XAS spectrum near the Cu edge is similar to that of square-planar Cu^{2+} in $BiCu_3Mn_4O_{12}$ (ref. 39), although satellite structures due to the charge-transfer screening process are seen in the present $CaCu_3Fe_2Re_2O_{12}$, and the Fe spectrum is similar to the typical $Fe^{3+}O_6$ signal in $LaFeO_3$ (ref. 40). The L_3-edge MCD intensities are negative for both Cu and Fe, and the L_2-edge intensities are positive for both metals—the coincident signs at each edge demonstrate that the spins of the A′-site Cu^{2+} and B-site Fe^{3+} ions couple ferromagnetically. The magnetic moments obtained from the MCD intensities by using magneto-optical sum rules[41,42] are 0.86 μ_B (spin part, 0.82 μ_B) for Cu and 4.17 μ_B (spin part, 4.11 μ_B) for Fe, in reasonably good agreement with the expected moments for Cu^{2+} ($S = 1/2$) and Fe^{3+} ($S = 5/2$). Analysis of preliminary powder neutron diffraction also supports the spin ordering model, as shown in Supplementary Fig. 1 and Supplementary Table 1.

The ferrimagnetic spin structure of $CaCu_3Fe_2Re_2O_{12}$ differs markedly from those of related cation-ordered perovskites, most notably in having ferromagnetic coupling between A′-site Cu^{2+} and the dominant B-site Fe^{3+} spins, as illustrated in Fig. 5. The double-perovskite Ca_2FeSbO_6 with nonmagnetic Sb^{5+} ions at the B′ sites shows spin-glass behaviour at low temperatures due to geometric frustration of antiferromagnetic interactions within the tetrahedral B sublattice of Fe^{3+} moments (Fig. 5a)[43]. Introducing Cu^{2+} at the A′ site to give $CaCu_3Fe_2Sb_2O_{12}$ relieves the spin frustration leading to ferrimagnetism below 170 K, but the Cu^{2+} spins couple antiferromagnetically with the B-site Fe^{3+} spins (Fig. 5b)[35]. This was confirmed by the MCD intensities of $CaCu_3Fe_2Sb_2O_{12}$, which are positive/negative at the Fe L_2/L_3-edges but negative/positive for Cu L_2/L_3-edges, in contrast to the spectra for $CaCu_3Fe_2Re_2O_{12}$ shown in Fig. 4. In charge-disproportionated $CaCu_3Fe_4O_{12}$ ($CaCu^{2+}{}_3Fe^{3+}{}_2Fe^{5+}{}_2O_{12}$), the Cu^{2+} spins at the A′ site also couple antiferromagnetically

Table 1 | Refined structure parameters of $CaCu_3Fe_2Re_2O_{12}$ at room temperature.

Atom	Site	*x*	*y*	*z*	*G*	U_{iso} (100 × Å^2)
Ca	2*a*	0.25	0.25	0.25	1.0	1.2 (2)
Cu	6*d*	0.25	0.75	0.75	1.0	0.39 (2)
Fe1	4*b*	0.0	0.0	0.0	0.938 (1)	0.22 (2)
Re1	4*b*	0.0	0.0	0.0	0.062	0.22
Fe2	4*c*	0.5	0.5	0.5	0.062	0.15 (1)
Re2	4*c*	0.5	0.5	0.5	0.938	0.15
O	24*h*	0.4496 (6)	0.7548 (5)	0.0691 (6)	1.0	0.37 (7)

Estimated s.d. of independent variables are shown in parentheses. Site occupation factors *G*; isotropic thermal parameters U_{iso}; space group: $Pn\bar{3}$ (no. 201); lattice parameter $a = 7.44664(3)$ Å; residuals $R_{wp} = 6.83\%$ and $\chi^2 = 2.45$.

Table 2 | M-O distances and BVS calculated for $CaCu_3Fe_2Re_2O_{12}$ from the structure analysis results in Table 1.

Atom	M-O (Å)	BVS
Ca	2.611 (5) × 12	2.10
Cu	2.006 (5) × 4	1.90
	2.803 (5) × 4	
	3.264 (5) × 4	
Fe	2.001 (5) × 6	3.12
Re	1.934 (5) × 6	4.91

BVS, bond valence sum; M, metal; O, oxygen.

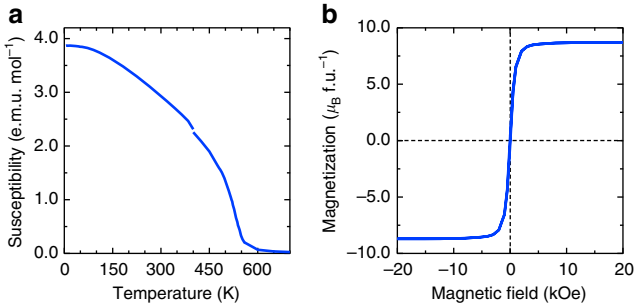

Figure 3 | Magnetic properties of $CaCu_3Fe_2Re_2O_{12}$. (**a**) Temperature dependence of magnetic susceptibility measured under an external field of 10 kOe, with the magnetic transition observed at 560 K. (**b**) Magnetization-field measurements at 5 K, revealing a large saturated magnetization of 8.7 μ_B f.u.$^{-1}$. The low-field region is expanded in Fig. 7b.

with B-site Fe^{3+} as well as with the B′-site Fe^{5+} spins (Fig. 5c)[38,44] and the ferrimagnetic spin structure stabilized below 210 K is different to that of $CaCu_3Fe_2Re_2O_{12}$ (Fig. 5d) regarding the B-site Fe^{3+} spin direction. A strong A′(Cu^{2+})–B′(Re^{5+}) antiferromagnetic interaction in $CaCu_3Fe_2Re_2O_{12}$ evidently outweighs the A′(Cu^{2+})–B(Fe^{3+}) interaction leading to ferromagnetic A′(Cu^{2+})–B(Fe^{3+}) spin alignment.

The $T_c = 560$ K of $CaCu_3Fe_2Re_2O_{12}$ is much greater than those of the materials shown in Fig. 5 or indeed of any 1:3 A-site-ordered perovskites reported to date. The very high Curie temperature of $CaCu_3Fe_2Re_2O_{12}$ is indicative of strong antiferromagnetic B(Fe^{3+})–B′(Re^{5+}) coupling, as ferrimagnetic A_2FeReO_6 double perovskites have comparable T_c's (of 520, 400 and 300 K for A = Ca, Sr and Ba, respectively)[22,45–48]. It is notable that $CaCu_3Fe_2Re_2O_{12}$ has a higher T_c than Ca_2FeReO_6 and a greater saturated magnetization (8.7 μ_B f.u.$^{-1}$ versus 4.7 μ_B (double f.u.)$^{-1}$ of Ca_2FeReO_6 (ref. 49)). A further difference is that $CaCu_3Fe_2Re_2O_{12}$ is a soft ferrimagnet with a coercive field of ~100 Oe and so is well-suited to low-field switching in spintronic devices, whereas Ca_2FeReO_6 is a hard magnetic material with a large coercivity of ≈10 kOe (refs 47,49). Magnetic anisotropy due to spin-orbit coupling of Re^{5+} is strongly coupled to the monoclinically distorted structure of Ca_2FeReO_6, whereas cubic $CaCu_3Fe_2Re_2O_{12}$ is more isotropic. A few double perovskites have higher Curie temperatures than $CaCu_3Fe_2Re_2O_{12}$, for example 600 K in Sr_2CrReO_6 and 725 K in Sr_2CrOsO_6, but these materials have far smaller saturated magnetizations, of 1.9 and 1.8 μ_B (double f.u.)$^{-1}$, respectively[22,50,51]. Hence, $CaCu_3Fe_2Re_2O_{12}$ is notable among magnetic oxides in offering both a high T_c and a large saturated magnetization.

Electronic structure and magnetotransport properties of $CaCu_3Fe_2Re_2O_{12}$. Spin-polarized electronic structure calculations

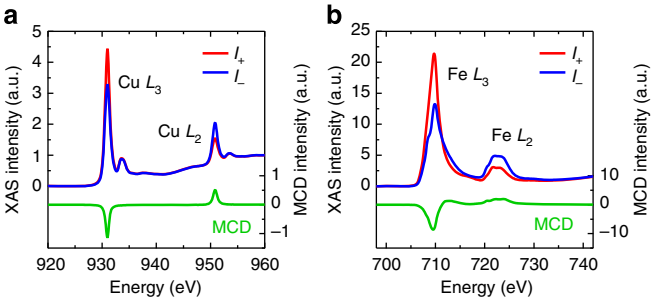

Figure 4 | XAS and MCD intensities of $CaCu_3Fe_2Re_2O_{12}$. (**a**) XAS and MCD intensities near the Cu L_3 and L_2-edges. (**b**) XAS and MCD intensities near the Fe L_3 and L_2-edges. Data were obtained at 15 K. The red and blue curves, respectively, represent XAS spectra measured with photon spins parallel (I_+) and antiparallel (I_-) to the magnetization direction of the sample, in which a static magnetic field of 19 kOe was applied. The MCD intensity was calculated as the difference between the I_+ and I_- absorption spectra. The coincident signs of the Cu and Fe MCD intensities at each L-edge show that their spins couple ferromagnetically.

converge to the observed ferrimagnetic $CaCu^{2+}(\uparrow)_3Fe^{3+}(\uparrow)_2Re^{5+}(\downarrow)_2O_{12}$ ground state irrespective of the initial spin structure, showing that this ground state is very stable. The total magnetic moment is 9.0 μ_B f.u.$^{-1}$ and the calculated magnetic moments inside the muffin-tin spheres for Cu, Fe and Re are respectively 0.39, 4.03 and −0.72 μ_B, which are slightly reduced from ideal 2S values due to strong hybridization with O 2p orbitals. An important prediction from the calculations is that $CaCu_3Fe_2Re_2O_{12}$ is half-metallic with fully spin-polarized conduction electrons, as shown in Fig. 6. The electronic band structure has a large gap in the up(majority)-spin bands and only down(minority)-spin bands of mainly Re 5d hybridized with O 2p states cross the Fermi level (E_F). In contrast, Ca_2FeReO_6 is predicted to be an insulator with gaps at E_F for both majority-spin and minority-spin bands and does not show metallic conductivity[47,52].

Resistivity and magnetoresistance measurements on a ceramic pellet of $CaCu_3Fe_2Re_2O_{12}$ are shown in Fig. 7. The resistivity is near 10 mΩ cm at room temperature and the observed slight increase on cooling (inset of Fig. 7a) would correspond to an unrealistically small gap energy of <1 meV if $CaCu_3Fe_2Re_2O_{12}$ was semiconducting. This suggests that grain boundary resistances mask the underlying metallic conductivity. The observed conducting behaviour of $CaCu_3Fe_2Re_2O_{12}$ is different from the insulating behaviour of $CaCu_3Fe_2Sb_2O_{12}$ (ref. 35) and the semiconductivity of charge-disproportionated $CaCu_3Fe_4O_{12}$ (ref. 38). Spin-polarized conduction is revealed by the decrease in low-temperature resistivity of the sample under magnetic fields with a sharp low-field magnetoresistance contribution at magnetic fields <3 kOe. This is indicative of spin-dependent tunnelling of spin-polarized conduction electrons through grain or domain boundaries[53]. Close inspection shows that the hysteresis in low-field magnetoresistance slightly differs from that in the magnetization, as the peak-to-peak magnetoresistance separation does not coincide with the coercive field value (Fig. 7b). The behaviour is similar to that observed in half-metallic Sr_2FeMoO_6 and suggests a spin-valve-type magnetoresistance due to the intergrain tunnelling of spin-polarized conduction carriers[54]. Although the observed magnetoresistance ratio of our ceramic $CaCu_3Fe_2Re_2O_{12}$ sample is small, most likely due to the slight Fe/Re antisite disorder and the effect of small (≈140 nm) B-cation-ordered domains as discussed for Sr_2FeMoO_6 (ref. 26), the low-field magnetoresistance indicates that conduction electrons are spin-polarized in the quadruple perovskite $CaCu_3Fe_2Re_2O_{12}$.

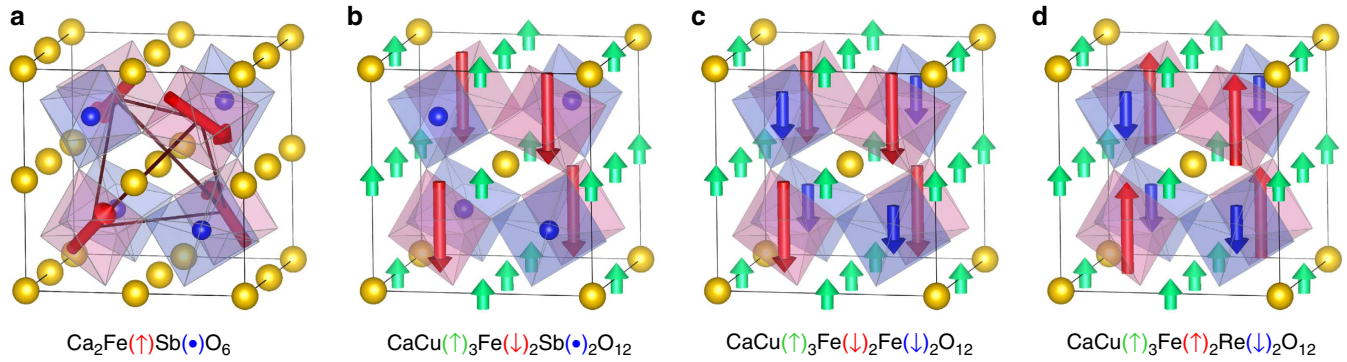

Figure 5 | Spin structures of perovskites with Fe^{3+} ions at cation-ordered B sites. (**a**) The double-perovskite Ca_2FeSbO_6 with a spin-glass transition temperature of 17 K. Order of antiferromagnetically interacting Fe^{3+} spins is frustrated due to the tetrahedral geometry of the B sublattice. (**b**) A- and B-site-ordered quadruple perovskite $CaCu_3Fe_2Sb_2O_{12}$ with nonmagnetic Sb^{5+} at the B′ site and $T_c = 170$ K. A′-site Cu^{2+} spins couple antiferromagnetically with the B-site Fe^{3+} spins. (**c**) Charge-disproportionated $CaCu_3Fe_4O_{12}$ with $T_c = 210$ K, where A′-site Cu^{2+} spins couple antiferromagnetically with the B-site Fe^{3+} and B′-site Fe^{5+} spins. (**d**) $CaCu_3Fe_2Re_2O_{12}$ where A′-site Cu^{2+} spins couple ferromagnetically with the B-site Fe^{3+} and antiferromagnetically with the B′-site Re^{5+} spins, leading to a high T_c of 560 K and a large magnetization of 8.7 μ_B f.u.$^{-1}$.

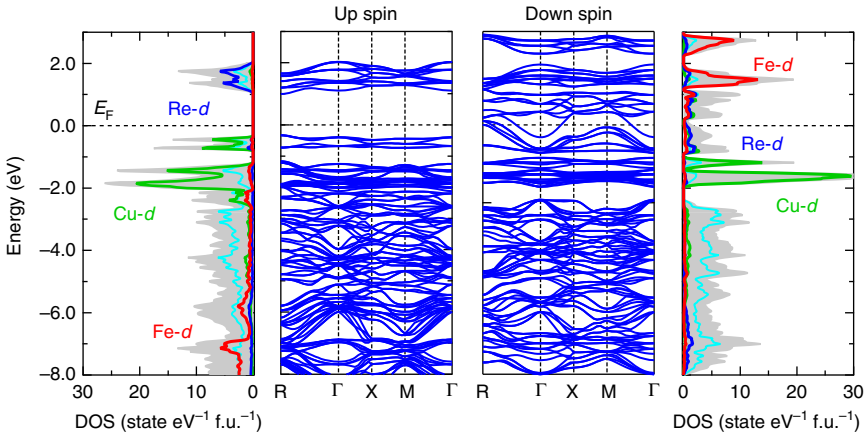

Figure 6 | Electronic structure of ferrimagnetic $CaCu_3Fe_2Re_2O_{12}$. Calculated density of states (DOS) and band structures for up-spin and down-spin electrons. Total DOS (shaded regions) and partial DOS of Cu (green curves), Fe (red curves), Re (blue curves) and O (light blue curves) are shown. Only the down(minority)-spin bands cross the Fermi level (E_F) as there is a gap in the up(majority)-spin bands. The calculation reproduces the $CaCu^{2+}(3d^9, S=1/2{:}\uparrow)_3Fe^{3+}(3d^5, S=5/2{:}\uparrow)_2Re^{5+}(5d^2, S=1{:}\downarrow)_2O_{12}$ ferrimagnetic spin structure well.

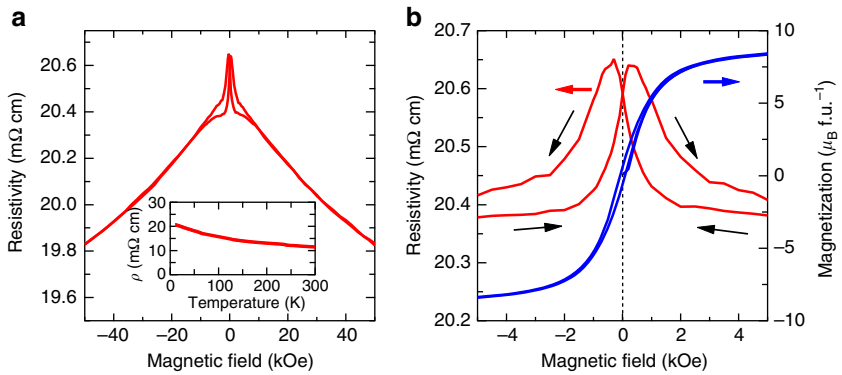

Figure 7 | Transport properties of $CaCu_3Fe_2Re_2O_{12}$. (**a**) Magnetic field dependence of resistivity measured at 10 K with external fields from −50 to 50 kOe. Inset shows temperature dependence of zero-field resistivity. (**b**) A magnified view of the field dependence of resistivity and magnetization on cycling. The observed low-field spin-valve-type magnetoresistance reveals intergrain tunnelling of spin-polarized conduction carriers.

Discussion

The new quadruple perovskite $CaCu_3Fe_2Re_2O_{12}$ synthesized by high-pressure and -temperature synthesis is cation ordered at both A and B sites, and has a cubic structure with formal charge distribution $Ca^{2+}Cu^{2+}{}_3Fe^{3+}{}_2Re^{5+}{}_2O_{12}$. Strong antiferromagnetic coupling of Re^{5+} spins to those of Cu^{2+} and Fe^{3+} results in ferrimagnetic $CaCu^{2+}(\uparrow)_3Fe^{3+}(\uparrow)_2Re^{5+}(\downarrow)_2O_{12}$ order with a high transition temperature (560 K) and a large magnetization

($8.7\ \mu_B$ f.u.$^{-1}$). XAS-MCD and neutron diffraction measurements confirm the ferrimagnetic spin structure. Electronic structure calculations predict that the ferrimagnetic ground state is half-metallic with only minority-spin bands crossing the Fermi level, producing highly spin-polarized conduction electrons. Resistivity measurements confirm spin-polarized conduction and a low-field spin-valve-type magnetoresistance is evident, although further optimization to suppress Fe/Re disorder fully is needed. The combination of a high magnetic ordering temperature and large magnetization, in comparison to double-perovskite analogues, and spin-polarized conductivity demonstrates that the introduction of further magnetic cations that can participate in a 1:3 order at the A sites is a good strategy for discovery of a new family of spintronic quadruple perovskite oxide materials.

Methods

Sample preparation. A polycrystalline sample of $CaCu_3Fe_2Re_2O_{12}$ was prepared by a solid-state reaction at a high temperature and high pressure. Stoichiometric amounts of $Ca_2Fe_2O_5$, CuO, Cu_2O, ReO_3 and Fe_2O_3 were well mixed and the mixture was sealed in a platinum capsule. The assembled sample cell was placed in a DIA-type cubic anvil high-pressure apparatus and treated at 10 GPa and 1400 K for an hour.

Crystal structure analysis. A SXRD experiment was carried out for phase identification and crystal structure analysis. The room-temperature SXRD pattern obtained with a wavelength of 0.498856 Å was recorded on the image plate of a large Debye–Scherrer camera installed at beamline BL02B2 in SPring-8. The powder sample was placed in a 0.1 mm glass capillary tube to minimize absorption and rotated during the measurement. The obtained data were analysed with the Rietveld method by using the TOPAS software package.

Magnetic and transport property measurements. Magnetic properties were measured with a commercial magnetometer (Quantum Design Magnetic Properties Measurement System). Temperature dependence of the magnetic susceptibility was measured at 5–700 K in an external magnetic field of 10 kOe. Field dependence of the magnetization was measured at several temperatures under fields ranging from -50 to 50 kOe. X-ray MCD spectra were obtained by a total electron yield method from X-ray absorption experiments conducted at beamline BL25SU in SPring-8. The powder sample was pasted uniformly on a sample holder by using carbon tape. The spectra at 15 K were obtained using parallel (I_+) and antiparallel (I_-) photon spins along the magnetization direction of the sample, to which a static magnetic field of 19 kOe was applied. The MCD intensity was defined as the difference between the two absorption spectra ($I_{MCD} = I_- - I_+$). Transport properties of the sample were measured in a conventional four-probe configuration. The temperature dependence of the resistivity and magnetoresistance were measured under magnetic fields ranging from -50 to 50 kOe.

Electronic structure calculation. The electronic structure of $CaCu_3Fe_2Re_2O_{12}$ was calculated by full-potential linearized augmented plane-wave first-principle calculations with the WIEN2k code. The lattice constant and atomic position parameters obtained from the structural refinement were used for the calculation. The full-potential linearized augmented plane-wave sphere radii for Ca, Cu, Fe, Re and O were respectively 2.0, 1.9, 1.9, 1.9 and 1.60 a.u. An effective U_{eff} ($= U - J$) of 4 eV was introduced for B-site Fe and B′-site Re. Self-consistency was carried out on 1000 k-point meshes in the whole Brillouin zone.

Neutron powder diffraction for magnetic structure analysis. Neutron powder diffraction from a $\sim$0.8 g polycrystalline $CaCu_3Fe_2Re_2O_{12}$ powder sample in a 5-mm-diameter vanadium was carried out using the D20 diffractometer at the Institut Laue-Langevin (ILL), Grenoble, France. The diffraction patterns were collected with a neutron wavelength of 2.4194 Å. The crystal and magnetic structures of data collected at 5 K were fitted by the Rietveld method using the General Structure Analysis System software package and the obtained results are shown in Supplementary Fig. S1 and Supplementary Table S1. Fe/Re inversion was not refined as these two elements have very similar nuclear scattering factors; b(Fe) = 9.5 fm and b(Re) = 9.2 fm.

References

1. Celotta, R. J. & Pierce, D. T. Polarized electron probes of magnetic surfaces. *Science* **234,** 333–340 (1986).
2. de Groot, R. A., Mueller, F. M., van Engen, P. G. & Buschow, K. H. J. New class of materials: half-metallic ferromagnets. *Phys. Rev. Lett.* **50,** 2024–2027 (1983).
3. Schwarz, K.-H. CrO_2 predicted as a half-metallic ferromagnet. *J. Phys. F Met. Phys.* **16,** L211–L215 (1986).
4. Wiesendanger, R., Güntherodt, H.-J., Güntherodt, G., Gambino, R. J. & Ruf, R. Observation of vacuum tunneling of spin-polarized electrons with the scanning tunneling microscope. *Phys. Rev. Lett.* **65,** 247–250 (1990).
5. Yanase, A. & Siratori, K. Band structure in the high temperature phase of Fe_3O_4. *J. Phys. Soc. Jpn* **53,** 312–317 (1984).
6. Shvets, I. V. *et al.* Progress towards spin-polarized scanning tunneling microscopy. *J. Appl. Phys.* **71,** 5489–5499 (1992).
7. Tokura, Y. *et al.* Giant magnetotransoprt phenomena in filling-controlled Kondo lattice system: $La_{1-x}Sr_xMnO_3$. *J. Phys. Soc. Jpn* **63,** 3931–3935 (1994).
8. Jin, S. *et al.* Thousandfold change in resistivity in magnetoresistive La-Ca-Mn-O films. *Science* **264,** 413–415 (1994).
9. Ramirez, A. P. Colossal magnetoresistance. *J. Phys. Condens. Matter* **9,** 8171–8199 (1997).
10. Shimakawa, Y., Kubo, Y. & Manako, T. Giant magnetoresistance in $Tl_2Mn_2O_7$ with the pyrochlore structure. *Nature* **379,** 53–55 (1996).
11. Jonker, G. H. & van Santen, J. H. Ferromagnetic compounds of manganese with perovskite structure. *Physica* **16,** 337–349 (1950).
12. Zener, C. Interaction between the d-shells in the transition metals. II. Ferromagnetic compounds of manganese with perovskite structure. *Phys. Rev.* **82,** 403–405 (1951).
13. de Gennes, P. G. Effects of double exchange in magnetic crystals. *Phys. Rev.* **118,** 141–154 (1960).
14. Pickett, W. E. & Singh, D. J. Electronic structure and half-metallic transport in the $La_{1-x}Ca_xMnO_3$ system. *Phys. Rev. B Condens. Matter* **53,** 1146–1160 (1996).
15. Park, J.-H. *et al.* Direct evidence for a half-metallic ferromagnet. *Nature* **392,** 794–796 (1998).
16. Sun, J. Z. *et al.* Observation of large low-field magnetoresistance in trilayer perpendicular transport devices made using doped manganate perovskites. *Appl. Phys. Lett.* **69,** 3266–3268 (1996).
17. Viret, M. *et al.* Low-field colossal magnetoresistance in manganite tunnel spin valves. *Europhys. Lett.* **39,** 545–549 (1997).
18. Obata, T., Manako, T., Shimakawa, Y. & Kubo, Y. Tunneling magnetoresistance at up to 270 K in $La_{0.8}Sr_{0.2}MnO_3/SrTiO_3/La_{0.8}Sr_{0.2}MnO_3$ junctions with 1.6-nm-thick barriers. *Appl. Phys. Lett.* **74,** 290–292 (1999).
19. Anderson, M. T., Greenwood, K. B., Taylor, G. A. & Poeppelmeier, K. R. B-cation arrangements in double perovskites. *Prog. Solid State Chem.* **22,** 197–233 (1993).
20. Howard, C. J., Kennedy, B. J. & Woodward, P. M. Ordered double perovskites—a group-theoretical analysis. *Acta Crystallogr. B* **59,** 463–471 (2003).
21. King, G. & Woodward, P. M. Cation ordering in perovskites. *J. Mater. Chem.* **20,** 5785–5796 (2010).
22. Serrate, D., De Teresa, J. M. & Ibarra, M. R. Double perovskites with ferromagnetism above room temperature. *J. Phys. Condens. Matter* **19,** 023201 (2007).
23. Saha-Dasgupta, T. Magnetism in double perovskites. *J. Supercond. Nov. Magn.* **26,** 1991–1995 (2013).
24. Kobayashi, K.-I., Kimura, T., Sawada, H., Terakura, K. & Tokura, Y. Room-temperature magnetoresistance in an oxide material with an ordered double-perovskite structure. *Nature* **395,** 677–680 (1998).
25. Meetei, O. N. *et al.* Theory of half-metallic double perovskites. I. Double exchange mechanism. *Phys. Rev. B* **87,** 165104 (2013).
26. Erten, O. *et al.* Theory of half-metallic double perovskites. II. Effective spin Hamiltonian and disorder effects. *Phys. Rev. B* **87,** 165105 (2013).
27. Vasil'ev, A. N. & Volkova, O. S. New functional materials $AC_3B_4O_{12}$ (Review). *Low Temp. Phys.* **33,** 895–914 (2007).
28. Shimakawa, Y. A-site-ordered perovskites with intriguing physical properties. *Inorg. Chem.* **47,** 8562–8570 (2008).
29. Shiraki, H. *et al.* Ferromagnetic cuprates $CaCu_3Ge_4O_{12}$ and $CaCu_3Sn_4O_{12}$ with *A*-site ordered perovskite structure. *Phys. Rev. B* **76,** 140403(R) (2007).
30. Shimakawa, Y., Shiraki, H. & Saito, T. Unusual ferromagnetic-to-antiferromagnetic-to-ferromagnetic transitions in Cu^{2+} ($S = 1/2$) cubic spin lattice of *A*-site ordered perovskites. *J. Phys. Soc. Jpn* **77,** 113702 (2008).
31. Zeng, Z., Greenblatt, M., Subramanian, M. A. & Croft, M. Large low-field magnetoresistance in perovskite-type $CaCu_3Mn_4O_{12}$ without double exchange. *Phys. Rev. Lett.* **82,** 3164–3167 (1999).
32. Alonso, J. A. *et al.* Enhanced magnetoresistance in the complex perovskite $LaCu_3Mn_4O_{12}$. *Appl. Phys. Lett.* **83,** 2623–2625 (2003).
33. Takata, K., Yamada, I., Azuma, M., Takano, M. & Shimakawa, Y. Magnetoresistance and electronic structure of the half-metallic ferrimagnet $BiCu_3Mn_4O_{12}$. *Phys. Rev. B* **76,** 024429 (2007).
34. Byeon, S.-H., Lee, S.-S., Parise, J. B., Woodward, P. M. & Hur, N. H. New ferrimagnetic oxide $CaCu_3Cr_2Sb_2O_{12}$: high-pressure synthesis, structure, and magnetic properties. *Chem. Mater.* **17,** 3552–3557 (2005).
35. Chen, W.-T., Mizumaki, M., Saito, T. & Shimakawa, Y. Frustration relieved ferrimagnetism in novel A- and B-site-ordered quadruple perovskite. *Dalton Trans.* **42,** 10116–10120 (2013).

36. Byeon, S.-H., Lee, S.-S., Parise, J. B. & Woodward, P. M. New perovskite oxide $CaCu_3Cr_2Ru_2O_{12}$: comparison with structural, magnetic, and transport properties of the $CaCu_3B_2B'_2O_{12}$ perovskite family. *Chem. Mater.* **18,** 3873–3877 (2006).
37. Brown, I. D. & Altermatt, D. Bond-valence parameters obtained from a systematic analysis of the Inorganic Crystal Structure Database. *Acta Crystallogr. B* **41,** 244–247 (1985).
38. Yamada, I. *et al.* A perovskite containing quadrivalent iron as a charge-disproportionated ferrimagnet. *Angew. Chem. Int. Ed.* **47,** 7032–7035 (2008).
39. Saito, T., Chen, W.-T., Mizumaki, M., Attfield, J. P. & Shimakawa, Y. Magnetic coupling between *A'* and *B* sites in the *A*-site-ordered perovskite $BiCu_3Mn_4O_{12}$. *Phys. Rev. B* **82,** 024426 (2010).
40. Abbate, M. *et al.* Controlled-valence properties of $La_{1-x}Sr_xFeO_3$ and $La_{1-x}Sr_xMnO_3$ studied by soft-X-ray absorption spectroscopy. *Phys. Rev. B* **46,** 4511–4519 (1992).
41. Thole, B. T., Carra, P., Sette, F. & van der Laan, G. X-ray circular dichroism as a probe of orbital magnetization. *Phys. Rev. Lett.* **68,** 1943–1946 (1992).
42. Carra, P., Thole, B. T., Altarelli, M. & Wang, X. X-ray circular dichroism and local magnetic fields. *Phys. Rev. Lett.* **70,** 694–697 (1993).
43. Battle, P. D., Gibb, T. C., Herod, A. J., Kim, S.-H. & Munns, P. H. Investigation of magnetic frustration in A_2FeMO_6 (A = Ca, Sr, Ba; M = Nb, Ta, Sb) by magnetometry and Mössbauer spectroscopy. *J. Mater. Chem.* **5,** 865–870 (1995).
44. Mizumaki, M. *et al.* Direct observation of the ferrimagnetic coupling of A-site Cu and B-site Fe spins in charge-disproportionated $CaCu_3Fe_4O_{12}$. *Phys. Rev. B* **84,** 094418 (2011).
45. Prellier, W. *et al.* Properties of the ferrimagnetic double perovskites A_2FeReO_6 (A = Ba and Ca). *J. Phys. Condens. Matter* **12,** 965–973 (2000).
46. Lofland, S. E. *et al.* Ferromagnetic resonance and magnetization studies on ferrimagnetic double perovskites A_2FeReO_6 (A = Ca, Sr, Ba). *IEEE Trans. Magn.* **37,** 2153–2155 (2001).
47. De Teresa, J. M., Serrate, D., Blasco, J., Ibarra, M. R. & Morellon, L. Impact of cation size on magnetic properties of $(AA')_2FeReO_6$ double perovskites. *Phys. Rev. B* **69,** 144401 (2004).
48. Wu, H. Electronic structure study of double perovskites A_2FeReO_6 (*A* = Ba, Sr, Ca) and Sr_2MMoO_6 (*M* = Cr, Mn, Fe, Co) by LSDA and LSDA + U. *Phys. Rev. B* **64,** 125126 (2001).
49. Alamelu, T., Varadaraju, U. V., Venkatesan, M., Douvalis, A. P. & Coey, J. M. D. Structural and magnetic properties of $(Sr_{2-x}Ca_x)FeReO_6$. *J. Appl. Phys.* **91,** 8909–8911 (2002).
50. Michalik, J. M. *et al.* High-field magnetization measurements in Sr_2CrReO_6 double perovskite: evidence for orbital contribution to the magnetization. *EPL* **78,** 17006 (2007).
51. Krockenberger, Y. *et al.* Sr_2CrOsO_6: end point of a spin-polarized metal-insulator transition by 5*d* band filling. *Phys. Rev. B* **75,** 020404 (2007).
52. Saitoh, T. *et al.* Strong electron correlation of Re 5d electrons in Ca_2FeReO_6. *J. Elec. Spec. Relat. Phenom.* **144-147,** 337–339 (2005).
53. Hwang, H. Y., Cheong, S. W., Ong, N. P. & Batlogg, B. Spin-polarized intergrain tunneling in $La_{2/3}Sr_{1/3}MnO_3$. *Phys. Rev. Lett.* **77,** 2041–2044 (1996).
54. Sarma, D. D. *et al.* Intergranular magnetoresistance in Sr_2FeMoO_6 from a magnetic tunnel barrier mechanism across grain boundaries. *Phys. Rev. Lett.* **98,** 157205 (2007).

Acknowledgements

We are grateful to J. Kim and N. Tsuji for their help with the SXRD measurements at BL02B2 in SPring-8, and to S. Zhang and N. Ichikawa for the transport measurements. Thanks are also to M. Tsujimoto, M. Toyoda and T. Oguchi for fruitful discussion on the electronic structure calculations. The SPring-8 experiments were performed with the approval of the Japan Synchrotron Radiation Research Institute (proposal nos: 2012A1006 and 2013B1011). This work was supported by Grants-in-Aid for Scientific Research (nos: 19GS0207 and 22740227), by a grant for the Joint Project of Chemical Synthesis Core Research Institutions from MEXT and by a JST-CREST program of Japan. Part of the work was performed under the Strategic Japanese-UK Cooperative Program by JST and ESPRC and under the young researchers exchange program of ICR, Kyoto University. Support was also provided by EPSRC, STFC and the Royal Society, UK.

Author contributions

W.-t.C. and Y.S. conceived and designed the study. W.-t.C., H.S., M.S.S., T.S. and D.K. prepared the sample and measured the structural and physical properties. M.M. performed the XAS-MCD experiments. Y.S. calculated the electronic structure. All of the authors contributed to the interpretation and discussion of the experimental results. W.-t.C., J.P.A. and Y.S. wrote the manuscript.

Additional information

Supplementary Information accompanies this paper at http://www.nature.com/naturecommunications

Competing financial interests: The authors declare no competing financial interests.

Reprints and permission information is available online at http://npg.nature.com/reprintsandpermissions/

How to cite this article: Chen, W.-t. *et al.* A half-metallic A- and B-site-ordered quadruple perovskite oxide $CaCu_3Fe_2Re_2O_{12}$ with large magnetization and a high transition temperature. *Nat. Commun.* 5:3909 doi: 10.1038/ncomms4909 (2014).